PID Controlling Approach Based on FBG Array Measurements for Laser Ablation of Pancreatic Tissues

Sanzhar Korganbayev, *Graduate Student Member, IEEE*, Annalisa Orrico, *Graduate Student Member, IEEE*, Leonardo Bianchi, *Graduate Student Member, IEEE*, Davide Paloschi, *Graduate Student Member, IEEE*, Alexey Wolf, Alexander Dostovalov, and Paola Saccomandi, *Senior Member, IEEE*

***Abstract*— In this article, we propose a temperature-based proportional–integral–derivative (PID) controlling algorithm using highly dense fiber Bragg grating (FBG) arrays for laser ablation (LA) of *ex vivo* pancreatic tissues. Custom-made highly dense FBG arrays with a spatial resolution of 1.2 mm were fabricated with the femtosecond point-by-point writing technology and optimized for LA applications. In order to obtain proper PID gain values, finite element method-based iterative simulation of different PID gains was performed. Then, the proposed algorithm, with numerically derived PID gains, was experimentally validated. In the experiments, the point temperature was controlled at different distances from the laser fiber tip (6.0, 7.2, 8.4, and 10.8 mm). The obtained results report robust controlling and correlation between controlled distance and the resulting area of ablation. The results of the work encourage further investigation of FBG array application for LA control.**

***Index Terms*— Closed-loop temperature control, feedback system, fiber Bragg grating (FBG) sensors, optical fiber, pancreas, proportional–integral–derivative (PID) control, temperature monitoring, thermal ablation (TA).**

I. Introduction

PANCREATIC ductal adenocarcinoma (PDAC) is the fourth cause of cancer deaths in the world, with about 57 600 new cases and 47 050 deaths in 2020 in the U.S. only [1]. This number is estimated to increase, and by 2030, PDAC will become the second leading cause of cancer-related deaths [2]. The main reasons for such statistics are difficulty in early diagnosis, high biological aggressiveness, and inefficiency of traditional approaches. Recently, thermal ablation (TA) techniques have received increasing interest in PDAC treatment due to their minimal invasiveness [3]. The main principle of these techniques is based on inducing local temperature change that leads to tumor necrosis. Depending on the source of temperature change, different ablation types exist—radio frequency, microwave, ultrasound, and laser ablation (LA) [4].

Among all ablation techniques, LA has unique advantages, such as flexibility and electromagnetic immunity of the fiber optic applicator, which allow the treatment of deep-lying organs under image guidance [5]. LA is based on the laser light absorption and scattering inside ablated tissue, which leads to temperature elevation and, consequently, to thermal damage of the treated tumor. For deep tumors, laser wavelengths in the so-called "therapeutic window" (940–1100 nm) are mostly utilized due to a good tradeoff between penetration depth and absorption of laser light by the tissue that entails the possibility to ablate large areas (tens of millimeters) [6].

However, the main limitation of LA, and other ablation techniques, is an uncertainty of the treatment results due to the complexity of the ablation phenomenon and the heat-tissue interactions [7], [8].

One of the possible solutions is a minimization of the uncertainty of the procedure by introducing a closed-loop approach based on measurements of intratissue parameters in the ablated region. One of the most important parameters to evaluate the efficacy of TA is temperature. Different ranges of temperatures have different effects on biological tissues. Temperatures from 42 °C to 45 °C correspond to hyperthermia and related activation of an immune response. At temperatures from 50 °C to 55 °C, coagulative necrosis of organs and instantaneous death in cell culture can be observed [7], whereas 60 °C is the starting temperature for rapid denaturation. As a result, accurate control of the desired temperature range is an important factor to ensure efficient cancer treatment.

It is worth noting that not only the tissue temperature value but also the time the tissue is exposed to this value are important to properly evaluate the thermal effect [8]. Thus, different models have been proposed to assess the thermal damage of TA techniques considering both these aspects. One of the models is the cumulative equivalent minutes at 43 °C (CEM43), which has been used to assess the severity of

Manuscript received August 11, 2021; accepted September 5, 2021. Date of publication September 20, 2021; date of current version September 29, 2021. This work was supported by the European Research Council through the European Union's Horizon 2020 Research and Innovation Program under Grant 759159. The work of Alexey Wolf and Alexander Dostovalov was supported by the Russian Ministry of Science and Higher Education under Grant 14.Y26.31.0017. The Associate Editor coordinating the review process was Yuya Koyama. *(Corresponding author: Paola Saccomandi.)*

Sanzhar Korganbayev, Annalisa Orrico, Leonardo Bianchi, Davide Paloschi, and Paola Saccomandi are with the Department of Mechanical Engineering, Politecnico di Milano, 20156 Milan, Italy (e-mail: sanzhar.korganbayev@polimi.it; annalisa.orrico@polimi.it; leonardo.bianchi@polimi.it; davide.paloschi@polimi.it; paola.saccomandi@polimi.it).

Alexey Wolf and Alexander Dostovalov are with the Department of Physics, Novosibirsk State University, 630090 Novosibirsk, Russia, and also with the Institute of Automation and Electrometry, Siberian Branch of the Russian Academy of Sciences, 630090 Novosibirsk, Russia (e-mail: wolf@iae.nsk.su; dostovalov@iae.nsk.su).

Digital Object Identifier 10.1109/TIM.2021.3112790

thermal damage for several tissue types [9]. In this regard, as will be discussed later in this article, the proposed LA regulation maintains controlling temperature at 43 °C during LA experiments.

The state-of-the-art works on temperature-based LA control mostly utilize traditional types of sensors: thermocouples [10], [11], and thermistor probes [12], [13]. The main disadvantages of these methods are the metallic material of the sensors and their low spatial resolution. Metallic material absorbs laser light and heat; thus leading to overestimation of temperature that can reach above 20 °C [14], [15]. The low spatial resolution of conventional sensors does not allow proper temperature reconstruction due to high thermal gradients, especially in the proximity of the applicator tip [8].

One of the possible alternatives to thermocouples and thermistors is the use of fiber Bragg grating (FBG) sensors. FBGs, as most optical sensors, are immune to electromagnetic interference, are small in size, and biocompatible. These advantages have led to increasing interest in FBG applications in LA treatments [16], [17].

Recently, our group has been working on FBG array applications for LA regulation using the ON–OFF controlling approach. The aim was the regulation of maximum temperature [18] and zone control [19] during contactless LA, and temperature control at different distances from the laser fiber tip during interstitial LA [20] of liver tissues. In order to improve controlling performance, in this article, we propose and experimentally validate a proportional–integral–derivative (PID)-based approach applied to the interstitial ablation of pancreatic tissue. In addition, the model of the heat transfer inside the tissue undergoing LA has been used for optimizing the choice of the PID parameters to be used in the experiments.

II. Materials and Methods

A. FBG Array Sensors

FBG is a periodic modulation of refractive index in the fiber core that behaves as a wavelength-dependent reflector, transmitting all wavelengths except the characteristic Bragg wavelength λ_B. The Bragg wavelength is proportional to the periodicity of modulation Λ

$$\lambda_{B=2} n_{\text{eff}} \Lambda \tag{1}$$

where n_{eff} is the effective refractive index of the core mode field.

The working principle of FBG relies on the fact that a temperature change ΔT alters Λ and n_{eff}, and, as a result, λ_B [21]

$$\frac{\Delta \lambda_B}{\lambda_B} = \alpha \cdot \Delta T \tag{2}$$

where α ($^\circ\text{C}^{-1}$) is the thermal sensitivity of the grating and $\Delta\lambda_B$ is the variation of λ_B.

Therefore, it is possible to reconstruct temperature changes along the FBG by measuring the $\Delta\lambda_\text{B}$ values. In addition, an array of FBGs along with the fiber (each FBG with different Λ and λ_B) can provide quasi-distributed temperature measurements, where each FBG acts as a sensing point.

A custom-made highly dense FBG array used in the experiments was fabricated with femtosecond point-by-point writing technology. The FBG array was inscribed in polyimide-coated single-mode fiber SM1500(9/125)P (Fibercore, Ltd., Southampton, U.K.) with a reduced coating diameter ($\sim$145 μm). For femtosecond point-by-point inscription, Pharos 6W (Light Conversion, Vilnius, Lithuania) femtosecond laser system producing pulses with a wavelength of 1026 nm and duration of 232 fs was utilized. ABL1000 (Aerotech, Inc., Pittsburgh, PA, USA) air-bearing linear stage was used for high-precision pulling of the fiber through the glass ferrule to set the position and individual resonant wavelength for each FBG in the array.

Pulling of the fiber with the predefined velocity (vi $\sim$ 1 mm/s) and simultaneous femtosecond irradiation with laser pulse sequence ($f = 1$ kHz) results in FBG inscription. The obtained Bragg wavelength is defined by $\lambda_{B,i} = 2n_{\text{eff}}\Lambda_i = 2n_{\text{eff}}v_i/mf$, where $m = 2$ is an order of FBG.

All 40 FBGs in the array were uniformly distributed in the spectral range of the used interrogator (1460–1620 nm) in order to reduce mutual interference of the neighboring gratings. Each of the gratings had a length of 1.15 mm, an edge-to-edge distance of 0.05 mm (the total length of the FBG array is 48 mm), and a uniform refractive index modulation profile, which gave us an FWHM spectral width of the grating of $\sim$700 pm. The reflection coefficient of an FBG in the range of 10%–20% allowed us to record the array reflection spectrum with a high dynamic range (>30 dB).

These FBG properties were optimized to have a narrow Bragg spectral width and at the same time to ensure accurate measurements of high-gradient temperature profiles that can reach up to 50 °C/mm near the applicator during LA procedures [8]. Moreover, the polyimide coating of the array provides the high thermal resistance (up to 400 °C) needed for accurate quasi-distributed measurements in this application [22]–[24]. The temperature sensitivity of the arrays is $(7.43 \pm 0.01) \times 10^{-6}$ $^\circ\text{C}^{-1}$. More information about the fabrication and the metrological characterization of the sensors can be found in the previous works of the group [19], [24].

The Micron Optics si255 optical interrogator (Micron Optics, Atlanta, USA, 1-pm accuracy, and wavelength range 1460–1620 nm) was utilized to measure the reflected spectra from the FBG arrays with a 100 Hz sampling rate.

B. Laser Ablation Equipment

Interstitial LA experiments were performed on *ex vivo* healthy porcine pancreatic tissue, which was obtained from a local farm. After the removal, the organs have been immediately placed in a sealed bag and stored in the fridge (4 °C). For the experiments, each specimen was prepared with a size suitable for placing in the custom-made box, which was used for accurate positioning of the sensor and laser fiber. The tissue temperature before the start of experiments was maintained at room temperature equal to 22 °C.

The diode laser (LuOcean Mini 4, Lumics, Berlin, Germany) working in continuous-wave mode at a 1064-nm

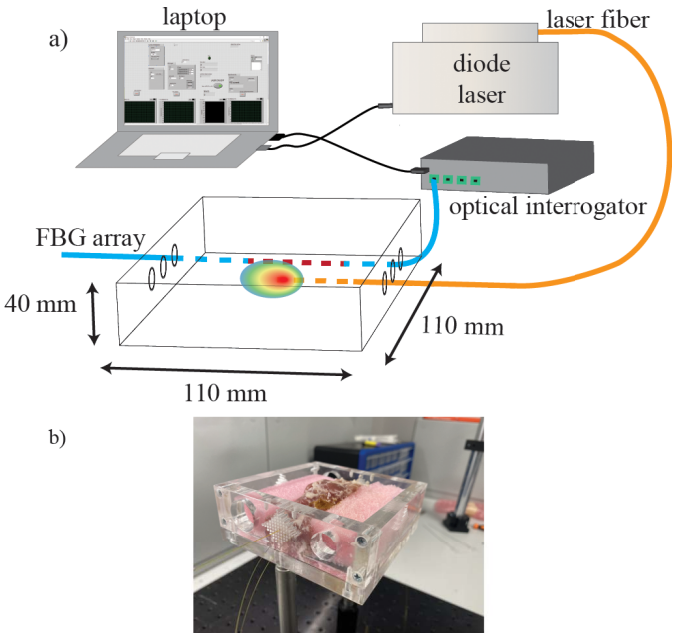

Fig. 1. (a) Schematics of the experimental setup: laser fiber and FBG array inserted in pancreatic tissue positioned in custom-made box; LA regulation setup consists of optical interrogator, diode laser, and laptop. (b) Photograph of sensors and laser fiber positioned in pancreatic tissue.

wavelength was used for ablation. This wavelength belongs to the "therapeutic window" largely used for assuring the overall absorption of the laser light by the biological tissues, thus, to entail the temperature increase necessary for the thermal therapy. It is worth noticing that 1064 nm is the wavelength that has been used for the first human trial on pancreatic tumors [25]. The flexible quartz optical fiber (300-μm diameter) was used to guide laser light inside the tissue.

The laser diode driver allows changing the output optical power via electrical current modulation during laser irradiation. For PID controlling, an electrical current range of 3000 (minimal current of the laser diode) to 8000 mA was chosen. In order to obtain corresponding power values, power was measured with a Newport 843-R-USB power meter (Newport Corporation, Irvine, CA, USA) for the current range selected. As a result, the obtained power range used for the PID temperature regulation experiments was 1.8–6.6 W.

C. Experimental Arrangement

The developed system consists of the laser diode and the interrogation system, both connected to a computer where a custom-made LabVIEW program was used to regulate LA.

A custom-made plexiglass box was employed to guarantee the accurate positioning of the laser fiber and sensors. The holes located on all sides of the box allow for different sensor and applicator arrangements in the tissue (Fig. 1).

The fibers were placed with the help of medical needles to prevent their damage during insertion into the pancreatic tissue. Initially, an 18-gauge needle (5-cm length) was inserted in the central hole of the lateral face of the box, and a 21-gauge needle (11-cm length) was inserted in a different hole at a

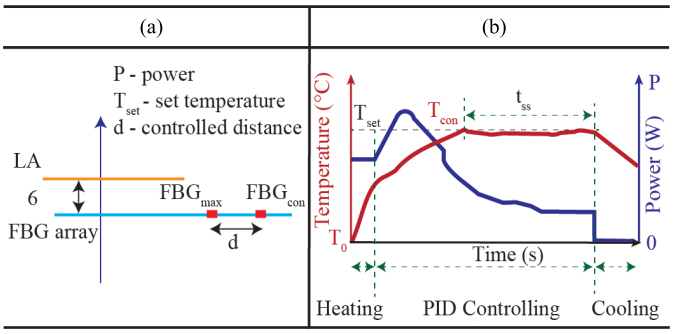

Fig. 2. Schematics of laser ablation algorithm. (a) Set of input parameters. (b) Schematics of controlled temperature evolution and related power during LA.

6-mm distance from the central one. Subsequently, the laser fiber and the FBG array fibers were inserted into the needles. The needles were then pulled out so that only the fibers remained inside the tissue.

The initial temperature of the pancreas, corresponding to 22.0 ± 0.5 °C, was measured with a thermocouple before each experiment. After experiments, the ablated volume was cut in the middle, and the axes of the ablated region were measured.

D. Controlling Algorithm

The developed LabVIEW program has two main phases (Fig. 2).

1) The input of preset parameters: set temperature T_{set}, PID gains, and d (distance between the grating with maximum temperature and the controlled grating).
2) Start of ablation with constant power (3.3 W) until a threshold of 10 °C of temperature change is reached. Then, the position of the grating exposed to the maximum temperature (FBG_{max}) is saved and position of the controlled grating (FBG_{con}) is calculated using the d value. After, regulation of the controlled temperature (T_{con}) at the controlled grating (FBG_{con}) is performed using the PID approach. Finally, after 300 s of steady-state time (t_{ss}), the laser is switched OFF.

E. Preplanning Model

In order to have an initial estimation of the gain coefficients of the PID controller, the heat-transfer phenomenon caused by the interaction between laser and the pancreas was simulated, along with the effects of the PID control.

The temperature distribution of an *ex vivo* biological tissue subjected to laser-induced thermal treatment is governed by the bio-heat transfer equation [26], expressed as

$$\rho \cdot c \cdot \frac{\partial T(t,r,z)}{\partial t} + \nabla(-k\nabla T(t,r,z)) = Q_{\text{source}} \qquad (3)$$

where $T(t,r,z)(K)$ is the tissue temperature, while the density, the specific heat, and the thermal conductivity of the biological tissue are represented with $\rho(\text{kg} \cdot \text{m}^{-3})$, $c(\text{J} \cdot \text{kg}^{-1}K^{-1})$, and $k(W \cdot m^{-1}K^{-1})$ respectively; the term $Q_{\text{source}}\left(W \cdot m^{-3}\right)$ represents the deposited thermal energy

TABLE I
PID GAINS FOR DIFFERENT SIMULATION SETS

	$k_p\,(A{\cdot}K^{-1})$	$k_i\,(A{\cdot}K^{-1}{\cdot}s^{-1})$	$k_d\,(A{\cdot}s{\cdot}K^{-1})$
Set 1	10	1	0
Set 2	1	10	5
Set 3	0.1	0.6	0
Set 4	0.7	0.006	0
Set 5	0.7	0	20

delivered by the laser source. Since the latter term is strongly affected by the light propagation in the tissue, a simple diffusion approximation method was employed to correctly predict the deposited thermal energy. The Beer–Lambert law [27] was used to predict the light propagation inside the tissue

$$\frac{\partial I(t,r,z)}{\partial z} = -\alpha_{\text{eff}} \cdot I(t,r,z). \tag{4}$$

The resulting deposited thermal energy [28] can be expressed as

$$Q_{\text{laser}} = \alpha_{\text{eff}} \cdot I_0(t,r) \cdot e^{-\alpha_{\text{eff}} \cdot z} \tag{5}$$

where $z(m)$ is the axial depth in tissue and $\alpha_{\text{eff}}(m^{-1})$ is the effective attenuation coefficient that was calculated based upon diffusion approximation [29] to consider both the absorption and the scattering phenomena. Lastly, $I_0(W{\cdot}m^{-2})$ represents the laser irradiance and is expressed as

$$I_0(t,r) = \frac{P(t)}{2\pi\sigma^2} \cdot e^{-\frac{r^2}{2\sigma^2}} \tag{6}$$

where $\sigma(m)$ is the standard deviation related to the beam profile, $r(m)$ is the radial distance, and $P(W)$ is the laser power that is linearly dependent on the laser current $C(A)$. This last parameter is set by a PID controller as follows:

$$C(t) = k_p \cdot (T_{\text{set}} - T_{\text{con}}) + k_i \cdot \int_0^t (T_{\text{set}} - T_{\text{con}}(\tau))d\tau + k_d \cdot \frac{d(T_{\text{set}} - T_{\text{con}}(t))}{dt}. \tag{7}$$

The PID controller maintains the temperature $T_{\text{con}}(K)$ at the same value of the setpoint temperature $T_{\text{set}}(K)$, upon a proper selection of the proportional $k_p(A{\cdot}K^{-1})$, integral $k_i(A{\cdot}K^{-1}{\cdot}s^{-1})$ and derivative $k_d(A{\cdot}s{\cdot}K^{-1})$ gain coefficients.

III. RESULTS AND DISCUSSION

A. Preplanning of PID Gains

The numerical model of the interstitial LA was solved using the finite element method (FEM)-based solver: COMSOL Multiphysics (COMSOL, Inc., Burlington, MA, USA). Several simulations were run to assess the best set of parameters for the PID controller based on the tissue thermal response. The tested gain coefficients are reported in Table I, and corresponding temperature profiles are reported in Fig. 3(a).

Fig. 3 shows the simulated thermal responses and the related output power profiles needed to achieve the setpoint temperature of 43 °C under five different PID settings at $d = 10.8$ mm. The output power profiles of Set 1, Set 2, and Set 3 experience abrupt changes when the controlled temperature approaches the setpoint value [Fig. 3(b)]. These PID sets do not possess control moderation and use mainly the minimum and maximum power available; consequently, they are not able to react in advance to the heat diffusion generated by a thermal gradient. As a result, they experience temperature overshoots and very lethargic setpoint tracking due to the suboptimal choice of the gains [Fig. 3(a)].

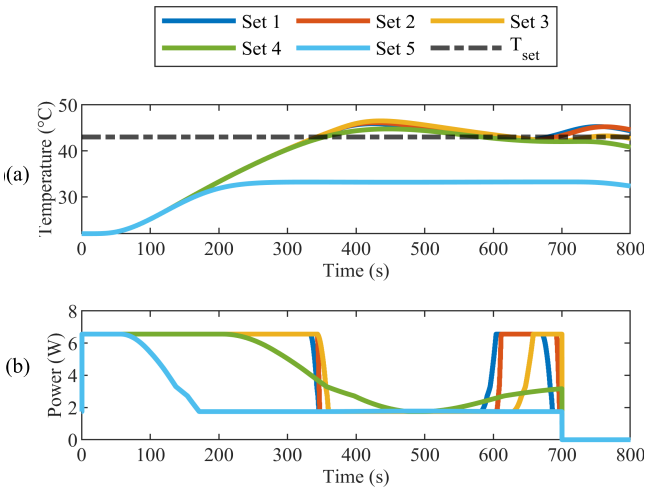

Fig. 3. Simulated temperature (a) and laser power (b) profiles for the different sets of PID gain values.

The light blue curve denotes the thermal response of the tissue temperature in the absence of the integral term in the PID system. Since k_i is responsible for enforcing zero steady-state error [30], the steady-state response of Set 5 is not able to reach the setpoint temperature. Conversely, the gain parameters selected in Set 4, i.e., $k_p = 0.7\ A \cdot K^{-1}, k_i = 0.006\ A \cdot K^{-1} \cdot s^{-1}$ and $k_d = 0\ A \cdot s \cdot K^{-1}$ showed a smoother power profile and a thermal response characterized by a rise time of ∼350 s and a smaller temperature overshoot of ∼1.8 °C (Fig. 3, green line). These last PID gain parameters were used for the experiments.

Robustness of selected PID gains for different controlled distances was checked by changing the position of the controlled point from $d = 10.8$ mm to $d = 7.2$ mm. Fig. 4 reports that the selected gains allow having a good controlling performance (i.e., rising time of ∼350 s and a temperature overshoot of ∼0.5 °C) also for $d = 7.2$ mm.

Fig. 5 shows the temperature distributions resulting from the LA regulation shown in Fig. 4 for $d = 10.8$ mm (Fig. 5 left-hand side) and $d = 7.2$ mm (right-hand side). Different thresholds were selected to display the volumes of pancreatic tissue subjected to specific temperatures, relevant for laser-assisted treatment purposes, in particular: 1) sublethal damage around T ∼ 43 °C; 2) instantaneous thermal damage for $T \geq 60$ °C; 3) vapor diffusion and tissue desiccation at $T \geq 100$ °C; and 4) removal of tissue mass for $T \geq 300$ °C [31]. As can be seen from Fig. 5, the controlled distance d affects the temperature distribution and, therefore, the extension of the thermal damage.

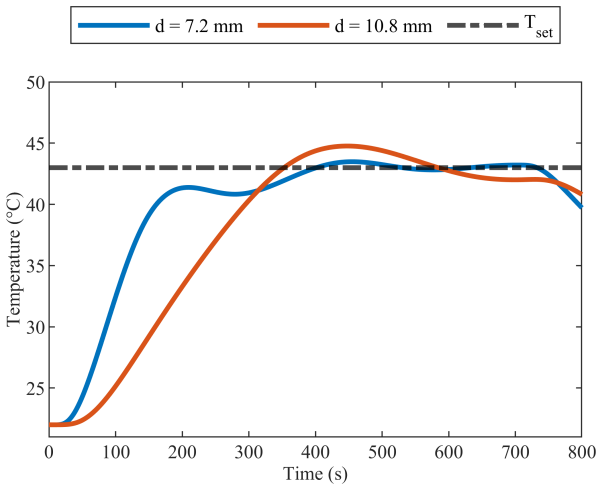

Fig. 4. Simulated controlled temperature profiles for different controlled distances.

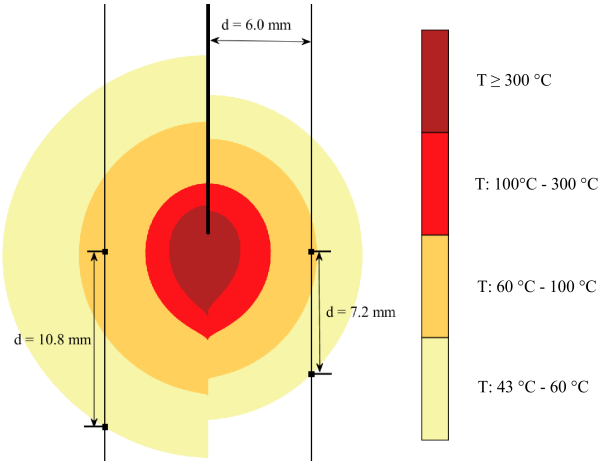

Fig. 5. Simulated temperature distributions for controlled distance equal to $d = 10.8$ mm (left) and $d = 7.2$ mm (right).

B. Experimental Results

After preplanning the PID controller and obtainment of the gain values, we used them for the experimental tests. In particular, experiments with different d values ($d = 6.0$, 7.2, 8.4, and 10.8 mm) were performed to further assess the robustness of the control strategy toward different distances and to validate the proposed LA regulation approach.

Fig. 6 reports the evolution of the controlled temperature and the laser power during LA of the pancreas. As it can be seen, the controlling algorithm allows for the proper regulation of the set temperature T_{set}, which was reached approximately after 350 s in all cases and maintained for $t_{ss} = 300$ s. Concerning the laser power, it is maintained constant for the first seconds of the procedure. Then, it suddenly changes to 5 W. For $d = 6.0$ and 7.2 mm, 5 W are maintained for ~100 s, whereas for $d = 10.8$ mm it is maintained for ~200 s. After this constant phase, the power decreases until it reaches another plateau at approximately 2 W. This plateau corresponds to the constant and desired temperature profile

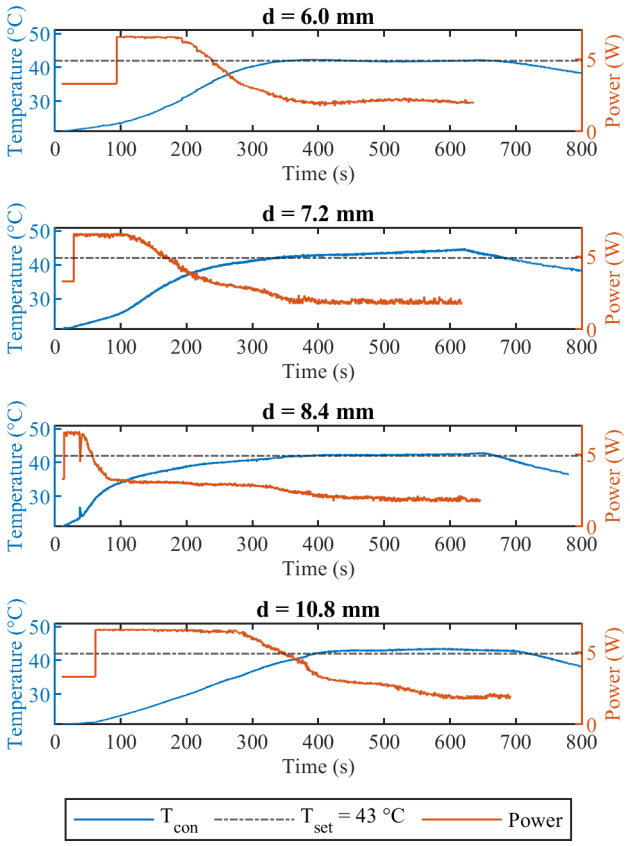

Fig. 6. Measured controlled temperature, set temperature (43 °C), and laser power profiles for different controlled distances.

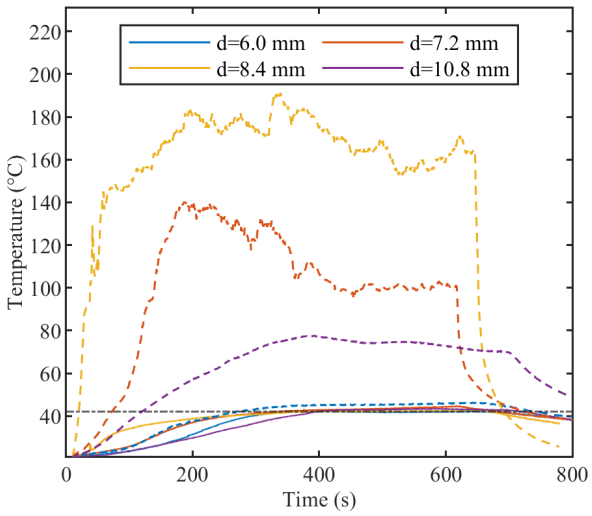

Fig. 7. Measured controlled temperature profiles (solid lines) and maximum measured temperature profiles (dashed lines) for different controlled distances.

measured in the tissue and achieved with the implemented control strategy.

Fig. 7 shows controlled temperatures for different d values and related maximum measured temperatures (dashed lines). Despite the high differences between controlled and maximum temperatures (up to 140 °C), the control has an overdamped behavior for all tests. The results shown in Fig. 7 further highlight the key role of the implemented control strategy for the

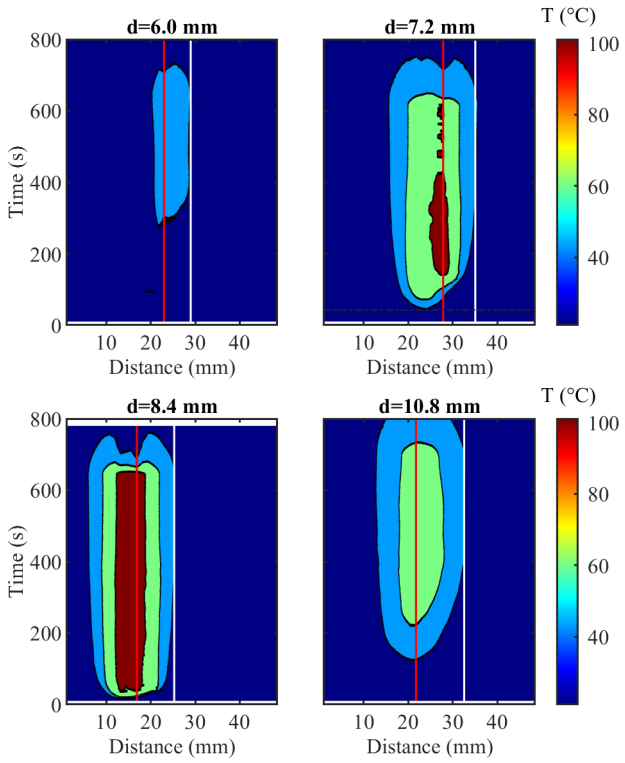

Fig. 8. Measured contour maps during laser ablation with different controlled distances for temperatures: 10 °C, 43 °C, 60 °C, and 100 °C. The red line shows the position of the FBG measuring the maximum temperature, and the white line depicts the position of the controlled grating.

application. Indeed, the complexity of the pancreas structure from the biological, optical, and thermal points of view causes irregular heat transfer in the organs, as demonstrated by the high and irregular maximum temperature profile measured on the FBGs of the array. Thus, the absence of a suitable control strategy can worsen the performance of the LA procedure.

The high spatial resolution of the highly dense FBG arrays allows for reconstructing temperature evolution maps (distance along with the array versus time) from the measured values, as shown in Fig. 8. The contour maps measured by the FBG array during laser ablation are depicted considering relevant temperatures for the LA biological outcome, i.e., 43 °C, 60 °C, and 100 °C. The red line shows the position of the FBG measuring the maximum temperature, and the white line depicts the position of the controlled grating. As can be seen from Fig. 9, the set temperature (43 °C contour) does not exceed the defined controlled distance (white line) for all tests. In addition, temperature contours can be used for the evaluation of instantaneous thermal damage ($T \geq 60$ °C) and vapor diffusion and tissue desiccation ($T \geq 100$ °C). We observe that for $d = 6.0$ mm, the FBG array experiences a temperature evolution which is maintained below 60 °C. This result is expected since the short control distance (with a set temperature of 43 °C) does not allow proper heat transfer in the tissue. For $d = 7.2$ mm, $d = 8.4$ mm, and $d = 10.8$ mm, the temperature is higher than the case of $d = 6.0$ mm, and at $d = 10.8$ mm, no contour at 100 °C is present. This result is also acceptable because the aim of the developed algorithm

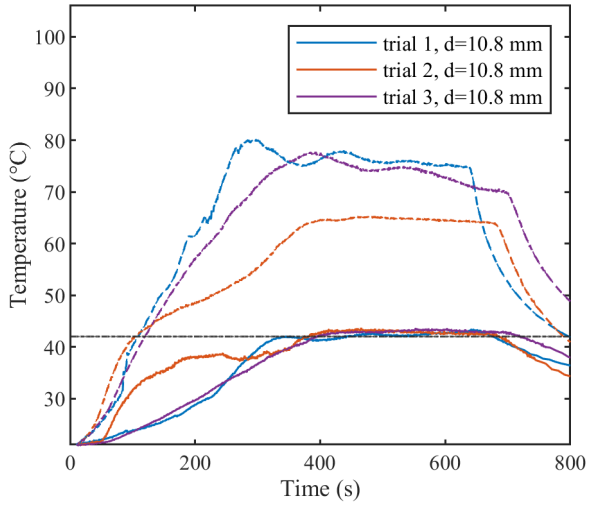

Fig. 9. Measured set temperature profiles (solid lines) and maximum temperature profiles (dashed lines) for the controlled distance of 10.8 mm.

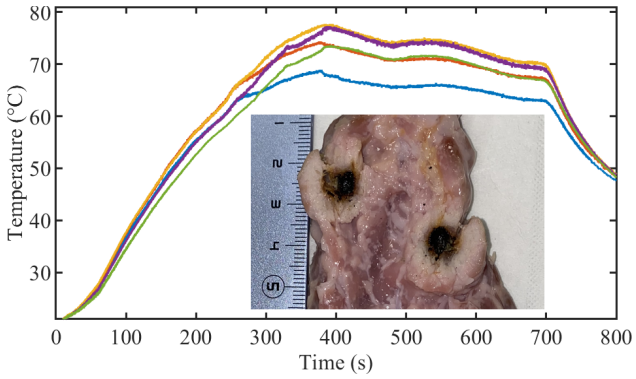

Fig. 10. Measured maximum temperature profile and profiles measured by adjacent gratings for controlled distance of 10.8 mm. Inset: Resulted ablated region of pancreatic tissue.

is to maintain the stable temperature at the controlled grating (white line in Fig. 8), while the maximum temperature can reach any value depending on laser-tissue interaction (as also shown in Fig. 7).

Fig. 9 shows the repeatability of the temperature control achievable with our approach. In this case, we report the maximum temperature profiles measured by the FBGs (dashed lines) and the controlled temperature measured by the FBG placed at $d = 10.8$ mm (continuous line). Three trials on different parts of *ex vivo* pancreatic tissue have been repeated, avoiding any overlap of the damaged zone between consecutive tests. As it can be seen, the control algorithm is able to maintain stable temperature during t_{ss} for all trials. The slight differences can be due to the inhomogeneity of the tissue.

Moreover, the high spatial resolution of the sensors can provide information about the thermal gradient. For instance, we observed that across an intragrating distance of about 2.4 mm, a temperature difference of ∼10 °C can be measured (Fig. 10), which proves the need for high-resolution sensors for such measurements.

The final results of LA control are presented in Table II. The energy of the treatment was calculated by using the laser power values used for PID control and the duration of the controlled

TABLE II
LA REGULATION RESULTS FOR DIFFERENT CONTROLLED DISTANCES

d (mm)	Time of PID regulation (s)	Energy (J)	Ablated dimensions (mm x mm)
6.0	541.7	1844	7.57 × 6.71
7.2	588.6	1943	12.07 × 8.03
8.4	631.8	1729	14.15 × 10.76
10.8	629.8	2695	17.39 × 14.11

ablation. Table II reports that the size of the ablated area mostly depends on controlled distance d and is less correlated with energy or time of ablation. As a result, the proposed LA regulation approach allows controlling the size of the ablated region by changing the controlled distance parameter.

The obtained experimental results validate the proposed PID approach for LA regulation and show the efficacy of FEM-based pre-experiment simulations to obtain effective PID gain values. However, limitations regarding the reliability of the simulations in the prediction of the final clinical outcome are represented by the lack of literature about the behavior of the thermo-optical pancreatic properties with respect to temperatures and by the complexity of photothermal-induced heat transfer in biological tissue. Thus, thermo-optical tissue properties need to be investigated in detail to improve TA simulations and their applications in tumor treatment.

In the proposed approach, temperature measurements performed by custom-made highly dense FBG arrays allow for efficient controlling of temperature at different distances and ablation volumes. The high spatial resolution and electromagnetic immunity of the used sensors provide unique advantages in comparison with traditional measurement techniques. Indeed, in the recent work focused on the PID regulation of LA based on thermocouple measurements, a 0.5-mm plastic plate was positioned between the laser applicator and the thermocouple to prevent laser light artifacts along with self-heating [30]. This approach significantly limits possible clinical applications of all of the standard temperature sensors for LA. For instance, the recent work of Paiella *et al.* [32] on clinical testing of immune-stimulating interstitial laser thermotherapy of the pancreas using a feedback mode with conventional sensors (thermistors) reports unsatisfactory results in terms of device handling, safety, and feasibility.

Thus, the limitations of convenient sensors observed in the literature encourage further investigation of fiber optic use for LA control. Indeed, recent investigations of single-FBG-based measurements for PID-based control were performed for a laser-heated needle for biopsy tract ablation and showed promising results [33], [34]. In addition, the use of highly dense FBG arrays for LA regulation has been discussed in the recent works of our group [18]–[20], where an ON–OFF control law yielded undesirable overshoots and delayed responses in the temperature regulation.

Nevertheless, one of the limitations of FBG array use for TA is the temperature-strain cross-sensitivity that can lead to measurement artifacts during temperature monitoring. In our experimental setup, this artifact was minimized using the difference between diameters of the needle utilized for FBG placing (21 G = 0.819 mm) and the FBG array diameter (145 μm). This difference results in slightly looser adhesion between tissue and the sensor, thus decreasing strain effect [35], [36].

In order to significantly reduce strain artifacts stemming from the axial strain and bending, a suitable embodiment [glass or polytetrafluoroethylene (PTFE) capillary] to encapsulate FBG needs to be developed. However, it can affect sensor dynamic response and absorb the part of the laser light during LA. As a result, more investigations need to be performed in the encapsulation development to completely avoid strain artifacts during FBG temperature measurements.

IV. CONCLUSION

In conclusion, a temperature-based feedback approach for LA regulation was investigated. For temperature measurements, custom-made highly dense FBG arrays were inscribed in single-core fiber using point-by-point writing technology. The high spatial resolution (1.2 mm) and temperature resistance above the typical maximum temperatures of LA provide unique advantages for thermometry. Moreover, FEM-based iterative simulations were developed to optimize the choice of PID gains. In order to validate the closed-loop approach, the point temperature was controlled at different distances from the laser fiber tip (6, 7.2, 8.4, and 10.8 mm). The approach here proposed is an innovative feature for the specific application of laser ablation for tumor treatment, where usually no control at all is performed, but the procedure relies only on the experience of the doctor. The results show effective temperature control for all distances and for all experimental trials. The results of the work encourage further investigation of FBG array applications for LA regulation.

REFERENCES

[1] R. L. Siegel, K. D. Miller, and A. Jemal, "Cancer statistics, 2020," *CA: A Cancer J. Clinicians*, vol. 70, no. 1, pp. 7–30, Jan. 2020, doi: 10.3322/caac.21590.

[2] L. Rahib, B. D. Smith, R. Aizenberg, A. B. Rosenzweig, J. M. Fleshman, and L. M. Matrisian, "Projecting cancer incidence and deaths to 2030: The unexpected burden of thyroid, liver, and pancreas cancers in the united states," *Cancer Res.*, vol. 74, no. 11, pp. 2913–2921, Jun. 2014.

[3] J. Han and K. J. Chang, "Endoscopic ultrasound-guided direct intervention for solid pancreatic tumors," *Clin. Endoscopy*, vol. 50, no. 2, pp. 126–137, Mar. 2017, doi: 10.5946/ce.2017.034.

[4] A. Ruarus, L. Vroomen, R. Puijk, H. Scheffer, and M. Meijerink, "Locally advanced pancreatic cancer: A review of local ablative therapies," *Cancers*, vol. 10, no. 1, p. 16, Jan. 2018.

[5] E. Schena, P. Saccomandi, and Y. Fong, "Laser ablation for cancer: Past, present and future," *J. Funct. Biomater.*, vol. 8, no. 2, p. 19, Jun. 2017, doi: 10.3390/jfb8020019.

[6] L. Bianchi *et al.*, "Thermal analysis of laser irradiation-gold nanorod combinations at 808 nm, 940 nm, 975 nm and 1064 nm wavelengths in breast cancer model," *Int. J. Hyperthermia*, vol. 38, no. 1, pp. 1099–1110, Jan. 2021.

[7] K. F. Chu and D. E. Dupuy, "Thermal ablation of tumours: Biological mechanisms and advances in therapy," *Nat. Rev. Cancer*, vol. 14, no. 3, pp. 199–208, 2014.

[8] A. J. Welch and M. J. C. Van Gemert, *Optical-Thermal Response of Laser-Irradiated Tissue*. Dordrecht, The Netherlands: Springer, 2011.

[9] P. S. Yarmolenko *et al.*, "Thresholds for thermal damage to normal tissues: An update," *Int. J. Hyperthermia*, vol. 27, no. 4, pp. 320–343, Jun. 2011, doi: 10.3109/02656736.2010.534527.

[10] J.-T. Lin, Y.-S. Chiang, G.-H. Lin, H. Lee, and H.-W. Liu, "In vitro photothermal destruction of cancer cells using gold nanorods and pulsed-train near-infrared laser," *J. Nanomater.*, vol. 2012, pp. 1–6, Jul. 2012, doi: 10.1155/2012/861385.
[11] J. T. Lin, "Selective cancer therapy using IR-laser-excited gold nanorods," *SPIE Newsroom*, vol. 2, no. 4, p. 2507, Feb. 2010, doi: 10.1117/12.841348.
[12] K. Ivarsson, J. Olsrud, C. Sturesson, P. H. Möller, B. R. Persson, and K.-G. Tranberg, "Feedback interstitial diode laser (805 nm) thermotherapy system: *Ex vivo* evaluation and mathematical modeling with one and four-fibers," *Lasers Surgery Med.*, vol. 22, no. 2, pp. 86–96, 1998.
[13] P. H. Möller, L. Lindberg, P. H. Henriksson, B. R. R. Persson, and K.-G. Tranberg, "Temperature control and light penetration in a feedback interstitial laser thermotherapy system," *Int. J. Hyperthermia*, vol. 12, no. 1, pp. 49–63, Jan. 1996, doi: 10.3109/02656739609023689.
[14] P. Saccomandi, E. Schena, and S. Silvestri, "Techniques for temperature monitoring during laser-induced thermotherapy: An overview," *Int. J. Hyperthermia*, vol. 29, no. 7, pp. 609–619, Nov. 2013, doi: 10.3109/02656736.2013.832411.
[15] F. Manns, P. J. Milne, X. Gonzalez-Cirre, D. B. Denham, J.-M. Parel, and D. S. Robinson, "*In situ* temperature measurements with thermocouple probes during laser interstitial thermotherapy (LITT): Quantification and correction of a measurement artifact," *Lasers Surgery Med.*, vol. 23, no. 2, pp. 94–103, 1998.
[16] A. Othonos, K. Kalli, and G. E. Kohnke, "Fiber Bragg gratings: Fundamentals and applications in telecommunications and sensing," *Phys. Today*, vol. 53, no. 5, p. 61, 2000.
[17] E. Udd and W. B. Spillman, Jr., *Fiber Optic Sensors: An Introduction for Engineers and Scientists*. Hoboken, NJ, USA: Wiley, 2011.
[18] S. Korganbayev, R. Pini, A. Orrico, A. Wolf, A. Dostovalov, and P. Saccomandi, "Towards temperature-controlled laser ablation based on fiber Bragg grating array temperature measurements," in *Proc. IEEE Int. Workshop Metrol. Ind. 4.0 (IoT)*, Jun. 2020, pp. 268–272.
[19] S. Korganbayev *et al.*, "Closed-loop temperature control based on fiber Bragg grating sensors for laser ablation of hepatic tissue," *Sensors*, vol. 20, no. 22, p. 6496, Nov. 2020.
[20] L. Bianchi, S. Korganbayev, A. Orrico, M. De Landro, and P. Saccomandi, "Quasi-distributed fiber optic sensor-based control system for interstitial laser ablation of tissue: Theoretical and experimental investigations," *Biomed. Opt. Exp.*, vol. 12, no. 5, p. 2841, May 2021, doi: 10.1364/BOE.419541.
[21] T. Erdogan, "Fiber grating spectra," *J. Lightw. Technol.*, vol. 15, no. 8, pp. 1277–1294, Aug. 15, 1997.
[22] K. T. V. Gratten and B. T. Meggitt, *Optical Fiber Sensor Technology*, vol. 3. Boston, MA, USA: Springer, 1998.
[23] L. Huang, R. S. Dyer, R. J. Lago, A. A. Stolov, and J. Li, "Mechanical properties of polyimide coated optical fibers at elevated temperatures," *Proc. SPIE*, vol. 9702, Mar. 2016, Art. no. 97020Y, doi: 10.1117/12.2210957.
[24] A. V. Dostovalov, A. A. Wolf, A. V. Parygin, V. E. Zyubin, and S. A. Babin, "Femtosecond point-by-point inscription of Bragg gratings by drawing a coated fiber through ferrule," *Opt. Exp.*, vol. 24, no. 15, pp. 16232–16237, 2016.
[25] P. Saccomandi, A. Lapergola, F. Longo, E. Schena, and G. Quero, "Thermal ablation of pancreatic cancer: A systematic literature review of clinical practice and pre-clinical studies," *Int. J. Hyperthermia*, vol. 35, no. 1, pp. 398–418, Dec. 2018, doi: 10.1080/02656736.2018.1506165.
[26] M. H. Niemz, *Laser-Tissue Interactions*, 3rd ed. Berlin, Germany: Springer, 2007.
[27] P. Saccomandi *et al.*, "Theoretical analysis and experimental evaluation of laser-induced interstitial thermotherapy in *ex vivo* porcine pancreas," *IEEE Trans. Biomed. Eng.*, vol. 59, no. 10, pp. 2958–2964, Oct. 2012, doi: 10.1109/TBME.2012.2210895.
[28] T. H. Nguyen, Y. H. Rhee, J. C. Ahn, and H. W. Kang, "Circumferential irradiation for interstitial coagulation of urethral stricture," *Opt. Exp.*, vol. 23, no. 16, pp. 20829–20840, Aug. 2015.
[29] A. Ishimaru, "Diffusion of light in turbid material," *Appl. Opt.*, vol. 28, no. 12, pp. 2210–2215, 1989, doi: 10.1364/AO.28.002210.
[30] T. H. Nguyen, S. Park, K. K. Hlaing, and H. W. Kang, "Temperature feedback-controlled photothermal treatment with diffusing applicator: Theoretical and experimental evaluations," *Biomed. Opt. Exp.*, vol. 7, no. 5, p. 1932, May 2016, doi: 10.1364/BOE.7.001932.
[31] A. J. Welch and M. J. C. Van Gemert, *Optical-Thermal Response of Laser-Irradiated Tissue*, vol. 2. Dordrecht, The Netherlands: Springer, 2011.
[32] S. Paiella *et al.*, "Laser treatment of pancreatic cancer with immunostimulating interstitial laser thermotherapy protocol: Safety and feasibility results from two phase 2a studies," *J. Surgical Res.*, vol. 259, pp. 1–7, Mar. 2021.
[33] H. H. Abd Raziff *et al.*, "A temperature-controlled laser hot needle with grating sensor for liver tissue tract ablation," *IEEE Trans. Instrum. Meas.*, vol. 69, pp. 7119–7124, 2020, doi: 10.1109/TIM.2020.2978920.
[34] H. H. A. Raziff *et al.*, "Laser-heated needle for biopsy tract ablation: *In vivo* study of rabbit liver biopsy," *Phys. Medica*, vol. 82, pp. 40–45, Feb. 2021, doi: 10.1016/j.ejmp.2021.01.067.
[35] L. Bianchi *et al.*, "Fiber Bragg grating sensors-based thermometry of gold nanorod-enhanced photothermal therapy in tumor model," *IEEE Sensors J.*, early access, May 19, 2021, doi: 10.1109/JSEN.2021.3082042.
[36] B. A. Patterson, D. D. Sampson, P. A. Krug, and S. K. Jones, "*In vivo* quasi-distributed temperature sensing with fibre Bragg gratings," in *Tech. Dig. Summaries papers Presented Conf. Lasers Electro-Opt. Postconf. Tech. Dig.*, May 2001, pp. 402–403.

Sanzhar Korganbayev (Graduate Student Member, IEEE) received the B.S. and M.S. degrees in electrical and electronics engineering from Nazarbayev University, Nur-Sultan, Kazakhstan, in 2016 and 2018, respectively. He is currently pursuing the Ph.D. degree with the Department of Mechanical Engineering, Politecnico di Milano, Milan, Italy.

He is currently involved in the LASER OPTIMAL Project (European Research Council Grant) for the development of software for real-time temperature monitoring and intraoperative adjustment of the laser ablation settings during tumor treatment. His research interests include fiber optic sensors and their applications for thermal and mechanical measurements.

Annalisa Orrico (Graduate Student Member, IEEE) received the B.S. and M.S. degrees in mechanical engineering from the Politecnico di Milano, Milan, Italy, in 2017 and 2020, respectively, where she is currently pursuing the Ph.D. degree with the Department of Mechanical Engineering.

She is currently involved in the HyperSIGHT project for the development of spectral imaging-based tools for the monitoring and prediction of thermal effects on tissues. Her research interest is the applications of imaging and fiber optic sensors for thermal measurements.

Leonardo Bianchi (Graduate Student Member, IEEE) received the M.Sc. degree (*cum laude*) in biomedical engineering from the Politecnico di Milano, Milan, Italy, in 2019, where he is currently pursuing the Ph.D. degree with the Department of Mechanical Engineering.

He is working in the framework of the LASER OPTIMAL project (European Research Council Grant) at the Politecnico di Milano. His research interests include the optimization of tumor laser ablation, from the numerical modeling and experimental assessment, nanoparticle-assisted photothermal therapies, and the related sensing techniques for temperature monitoring during treatments.

Davide Paloschi (Graduate Student Member, IEEE) received the B.S. and M.S. degrees in automation and control engineering from the Politecnico di Milano, Milan, Italy, in 2016 and 2018, respectively, where he is currently pursuing the Ph.D. degree with the Department of Mechanical Engineering.

From 2019 to 2020, he was a Research Fellow with the Department of Mechanical Engineering, Politecnico di Milano. His research interests include the monitoring of physiological parameters, model prediction, data analysis, and noise filtering.

Alexey Wolf received the M.Sc. degree in physics from Novosibirsk State University (NSU), Novosibirsk, Russia, and the Ph.D. degree in optics from the Institute of Automation and Electrometry, Siberian Branch of the Russian Academy of Sciences (IAE SB RAS), Novosibirsk, in 2013 and 2020, respectively.

He is currently a Researcher with the Laboratory of Nonlinear Waveguide Systems, NSU, and the Laboratory of Fiber Optics, IAE SB RAS, where he is involved in developing new types of fiber lasers and sensors based on specialty optical fibers. His scientific interests include femtosecond laser micromachining, fiber Bragg gratings, and new optical materials.

Alexander Dostovalov received the M.Sc. degree in physics from Novosibirsk State University (NSU), Novosibirsk, Russia, and the Ph.D. degree in optics from the Institute of Automation and Electrometry (IAE), Siberian Branch of the Russian Academy of Sciences, in 2009 and 2015, respectively.

Since 2018, he has been a Senior Research Fellow with IAE and the Laboratory of Nonlinear Waveguide Systems, NSU. He has authored more than 35 articles and five inventions. His research interests include femtosecond laser micromachining, fiber Bragg gratings inscription, fiber lasers, and sensors.

Paola Saccomandi (Senior Member, IEEE) received the Ph.D. degree in biomedical engineering from the Università Campus Bio-Medico di Roma, Rome, Italy, in 2014.

From 2016 to 2018, she was a Post-Doctoral Researcher with the IHU Strasbourg—Institute of Image-Guided Surgery of Strasbourg, Strasbourg, France. Since 2018, she has been an Associate Professor with the Department of Mechanical Engineering, Politecnico di Milano, Milan, Italy. She is a Principal Investigator of the European Research Council grant LASER OPTIMAL. Her main research interests include fiber optic sensors, biomedical imaging, and the development of light-based approaches for hyperthermal tumor treatment and monitoring.